Influence of excitons and electric fields on the dielectric function of GaN: Theory and experiment

A. T. Winzer, G. Gobsch, and R. Goldhahn*
Institut für Physik, TU Ilmenau, PF 100565, 98684 Ilmenau, Germany

D. Fuhrmann and A. Hangleiter
Institut für Angewandte Physik, TU Braunschweig, Mendelssohnstraße 2, 38106 Braunschweig, Germany

A. Dadgar and A. Krost
Institut für Experimentelle Physik, Otto-von-Guericke-Universität Magdeburg, PF 4120, 39016 Magdeburg, Germany
(Received 12 June 2006; revised manuscript received 31 July 2006; published 26 September 2006)

The shape of the complex dielectric function (DF) of nitride semiconductors in the vicinity of the band gap is strongly influenced by the electron-hole interaction (excitonic effects). Here, the influence of electric fields on the optical response is theoretically studied and compared to experimental data. An exact and numerically fast method is presented allowing the calculation of the imaginary part of the DF in the whole range of reasonable field strengths F. The real part of the DF is calculated via the Kramers-Kronig transformation. We discuss how the field influences position, magnitude, and broadening of the ground-state excitonic resonance as well as the absorption far below the band gap. In contrast to the one-electron picture, a linear increase of the energy position of the ground-state resonance is obtained for large F values. Electroreflectance (ER) spectroscopy carried out on an AlGaN/GaN heterojunction at low temperature demonstrates the sensitivity of the optical response to field changes. Using the calculated field-dependent values of the DF, the ER spectra of both the GaN channel layer and the AlGaN barrier layer are fully reproduced despite the inhomogeneous field distribution. The excellent agreement emphasizes the theoretical approach.

DOI: 10.1103/PhysRevB.74.125207 PACS number(s): 71.35.Cc, 78.20.Jq, 78.20.Bh, 78.20.Ci

I. INTRODUCTION

Exciton spectroscopy has been proven as a powerful tool for studying the fundamental properties of nitride semiconductors. For wurtzite GaN, high-resolution reflectance measurements of homoepitaxial films at liquid helium temperature[1] yielded the strain-free excitonic transition energies for the discrete states with Γ^5 symmetry that are optically active to light with the electric field vector polarized perpendicular to the optical (c) axis. These states are usually labeled with FX^A, FX^B, and FX^C and are constructed from the split valence bands with Γ^9, Γ^7, and Γ^7 symmetry, respectively, and the Γ^7 conduction band.[2] Adopting the hydrogen model, Rydberg energies R_y of 24.8 meV (A), 24.7 meV (B), and 26.8 meV (C) were determined from the energy splitting between the ground state ($n=1$) and the first excited state ($n=2$) transitions.[1]

However, almost all nitrides are heteroepitaxially grown on foreign substrates. Because of the mismatch in the lattice constants and/or in the thermal expansion coefficients, the deposited layers are strained, giving rise to a characteristic peak shift of the free excitonic lines compared to the strain-free values and a redistribution of oscillator strength between the B and C transitions.[2] Both effects are commonly used to evaluate the strain state of films, whereas the extracted exciton broadening energy is considered as a measure for the structural quality.

Thus far, the influence of electric fields on the shape of the excitonic absorption edge has been mostly disregarded in the discussion of experimental data. The main obstacle is that the effect cannot be described in analytical form; it requires extensive numerical calculations. The problem is formally equivalent to the Schrödinger equation for a hydrogen atom in an electric field of strength F. The most important parameter is the ratio of F to the classical ionization field strength F_{ion} (corresponding to a potential drop of R_y over the exciton Bohr radius a). A useful approach, how to calculate the photon energy ($\hbar\omega$) dependence of the imaginary part $\varepsilon_2(\hbar\omega,F)$ of the complex dielectric function (DF) $\hat{\varepsilon}(\hbar\omega,F)=\varepsilon_1(\hbar\omega,F)+i\varepsilon_2(\hbar\omega,F)$ for any semiconductor around the band gap, has already been reported by Blossey[3] and Dow and Redfield,[4] in 1970. An exact numerical solution for treating electron-hole interaction under applied electric fields is obtained by a transformation of the problem into parabolic coordinates. The calculations of ε_2 as function of F yielded the following features: (i) the main excitonic resonance (bound state) undergoes a nonmonotonic peak shift, (ii) its magnitude decreases with increasing F and merges with the exciton continuum at high fields, (iii) the field-induced absorption far below the band gap is several orders of magnitude larger compared to the classical one-electron Franz-Keldysh effect.[4]

Because of the large R_y and small a values, F_{ion} of GaN amounts to ~90 kV/cm, which is about 17–20 times larger than for the intensively studied GaAs.[5] Therefore, the aforementioned peculiarities should be much more pronounced for the nitride compound. Absorption measurements reported by Trautman *et al.*[6] and Shokhovets *et al.*[7] have shown the increase of broadening and the decrease of the bound exciton peak height at the GaN fundamental absorption edge in the presence of strong electric fields. Oberhofer *et al.*[8] used this effect for the demonstration of a light modulation device. Binet *et al.*[9] found an exciton peak shift in the absorption coefficient $\alpha(\hbar\omega,F)$ of high-quality GaN layers, although

 ©2006 The American Physical Society

their measurements were restricted to only small fields ($0 < F < 0.4F_{ion}$) applied lateral to the surface. For the quantitative interpretation of the spectra, it was assumed that $\alpha(\hbar\omega,F) \sim \varepsilon_2(\hbar\omega,F)$ holds. However, both quantities are related by

$$\alpha(\hbar\omega,F) = \frac{\omega\varepsilon_2(\hbar\omega,F)}{c_0 n(\hbar\omega,F)} = \frac{2\omega}{c_0}\Im[\sqrt{\hat{\varepsilon}(\hbar\omega,F)}], \quad (1)$$

where c_0 is the vacuum speed of light. Especially at excitonic resonances, it cannot be assumed that the refractive index $n(\hbar\omega,F)$ is a constant.

In this paper, we present a comprehensive theoretical and experimental investigation of the influence of electric fields on the excitonic DF of nitride semiconductors. Having introduced the fundamental relations, a method is described in Sec. II that requires low computational resources for the calculation of both ε_2 and ε_1. Electroreflectance (ER) spectroscopy at low temperature (T=5 K) on AlGaN/GaN heterostructures is applied in order to evidence the direct optical response of the excitonic DF to a change of F, details of the setup used are given in Sec. III. Experimental data for small F up to several F_{ion} are presented in Sec. IV. The theoretical results are used in order to model the GaN and AlGaN spectra over the whole field strength range. Section V summarizes the results.

II. THEORY

We consider absorption of a photon of energy $\hbar\omega$ by the creation of a Wannier exciton at a three-dimensional M_0 critical point of the band structure as described in detail in Ref. 3. There, it is assumed that (i) only one conduction and one nondegenerate valence band participate; (ii) the conduction band is empty and the valence band is completely filled; (iii) the bands are isotropic and parabolic; (iv) the electron and the hole in the final state interact via the Coulomb potential, exchange is neglected although for GaN the interaction energy may be as high as $0.15R_y$.[2] Using the results of Ref. 10, the increase of the reduced effective mass amounts to only 7% at 300 meV above E_g of GaN. This low nonparabolicity allows us to carry out all calculations in the parabolic band approximation (Blossey's approach) in order to demonstrate the principal behavior. Because of (i) we treat the three valence bands of GaN separately and add their individual contributions afterward, ignoring the mixing of the valence bands outside of the Brillouin zone center.[11]

In the following, the properties of the ordinary dielectric tensor component, corresponding to light polarization perpendicular to the optical (c) axis, will be discussed in detail. Note, the field influence on the extraordinary component is similar. At first $\varepsilon_2(\hbar\omega)$ is determined and $\varepsilon_1(\hbar\omega)$ is obtained by the Kramers-Kronig relation.[12]

A. Evaluation of Blossey's model

The calculation starts from Elliott's[13] expression for the imaginary part of the DF in the presence of electron-hole interaction,

$$\varepsilon_2(\hbar\omega) = \left(\frac{\pi e^2}{\varepsilon_0 m_0^2\omega^2}|M|^2\right)\sum_n 2|\phi_n(0)|^2\delta(E_g + E_n - \hbar\omega), \quad (2)$$

where e, ε_0, m_0, and E_g are the elementary charge, the vacuum dielectric constant, the free electron mass, and the gap energy, respectively. M is the momentum matrix element connecting the Bloch functions of the valence and the conduction band; it is assumed to be energy independent. The sum is evaluated over all states n with the wave functions $\phi_n(\mathbf{r})$ and the eigenenergies E_n satisfying the effective mass Schrödinger equation in coordinates of the electron-hole relative motion $\mathbf{r}$,

$$\left[-\frac{\hbar^2}{2\mu}\nabla^2 - \frac{e^2}{4\pi\varepsilon_0\varepsilon_r|\mathbf{r}|} - eFz\right]\phi_n(\mathbf{r}) = E_n\phi_n(\mathbf{r}), \quad (3)$$

where μ,ε_r are the reduced effective mass and the relative static dielectric constant, respectively. F is the static electric field with a component only in $\mathbf{r}=(0,0,z)$ direction.

By separation into parabolic coordinates and taking into account only wave functions that contribute to allowed transitions, Blossey reduced Eq. (3) to a pair of dimensionless differential equations of one variable x (x is not a real-space coordinate):

$$\frac{1}{x}\frac{d}{dx}\left(x\frac{d}{dx}\begin{bmatrix} f \\ g \end{bmatrix}\right) + \left(-\frac{1}{x}\begin{bmatrix} \varkappa \\ \varkappa' \end{bmatrix} + \beta - x\right)\begin{bmatrix} f \\ g \end{bmatrix} = 0, \quad \begin{bmatrix} x>0 \\ x<0 \end{bmatrix}. \quad (4)$$

The eigenvalues $\varkappa$ and $\varkappa'$ connect both equations by $\varkappa' = \varkappa + 2(F_{ion}/F)^{1/3}$. The transition energy is introduced by the dimensionless parameter $\beta = (F/F_{ion})^{-2/3}(E_n/R_y)$.

Generally, the sum over all n in Eq. (2) can be expressed by

$$\sum_n 2|\phi_n(0)|^2\delta(E_g + E_n - \hbar\omega) = \frac{\phi^2(0)}{2\pi^2 R_y a^3}, \quad (5)$$

where $\phi^2(0)$ is a dimensionless but field-dependent density of states parameter. This parameter is calculated from the properly normalized functions $f(x)$ and $g(x)$ via

$$\phi^2(0) = \left(\frac{F}{F_{ion}}\right)^{1/3}\sum_{i=1}^{\infty} f_{\varkappa_i}^2(0)g_{\varkappa_i'}^2(0). \quad (6)$$

The solutions of Equation (4) are labeled by the discrete set of the quantum number i, which is for bound states related to the orbital quantum number of the hydrogen atom.[3]

Eq. (4) was solved using the software package MATHEMATICA.[14] Our first step was the forward integration of f for $x>0$. The solutions $f_{\varkappa_i}(x)$ and $\varkappa_i$ form a set of functions that are discrete in the quantum number i and continuous in the dimensionless energy β. They were computed by a combination of the shooting method[15] and a Runge-Kutta method for a certain i and a certain β, starting from $x\to 0$ with arbitrary $f_{\varkappa_i}$ and $df/dx = \varkappa_i f_{\varkappa_i}$ according to l'Hospital's rule. The computation was carried out until a variation of $\varkappa_i$ yielded a sufficient exponential decay according to the asymptotic solution

$$f_{\varkappa_i,\beta}(x) \sim (x-\beta)^{-3/4} \exp\left[-\tfrac{2}{3}(x-\beta)^{3/2} + \varkappa_i(x-\beta)^{-1/2}\right]. \quad (7)$$

Good starting values for the $\varkappa_i$ are obtained by the Wentzel-Kramers-Brillouin approximation.[3] The numerical normalization leads then to $f^2_{\varkappa i,\beta}(0)$. Because this step has to be repeated for every energy β of a spectrum, it would require a huge amount of computational resources. Instead, it is feasible to store $f^2_{\varkappa i,\beta}(0)$ and $\varkappa_i$ as tabulated functions in a sufficiently large range of β for a series of i.

The next step is the backward integration of g for $x<0$ for a certain energy β and a certain eigenvalue $\varkappa_i' = \varkappa_i + 2(F_{ion}/F)^{1/3}$ in a similar manner as for f. Blossey[3] pointed out that it is not possible to normalize g by machine. Instead, one uses the property that the oscillatory asymptotic solution

$$g_{\varkappa_i',\beta}(x) \sim (-x+\beta)^{-3/4} \times \sin\left[\tfrac{2}{3}(-x+\beta)^{3/2} + \varkappa_i'(-x+\beta)^{1/2} + \alpha\right], \quad (8)$$

is already normalized in the sense of Eq. (6), where α is an arbitrary phase angle. Since we are only interested in the scaling, it is feasible to compare the envelope of the numerical solution with the asymptotic one. The function $g^2_{\varkappa_i',\beta}(0)$ contains sharp pikes for $\beta<0$ and $\varkappa_i'>0$, which are related to bound excitonic transitions showing up in ε_2 below the band gap at $F \ll F_{ion}$. For $\beta>0$, however, $g^2_{\varkappa_i',\beta}(0)$ is a smooth function and a tabulation in this range can reduce computational effort further.

With this, the F-dependent ε_2, according to Eqs. (2), (5), and (6), is obtained as presented for a few cases in Fig. 1. The curves have been broadened by a Gaussian line-shape function with a broadening parameter of $\Gamma=0.2R_y$. For $F=0.1F_{ion}$, a strong feature occurs below $E_n=0$ and a continuum part above $E_n=0$ ($E_n=0$ corresponds to E_g). When F is increased to $F=0.3F_{ion}$, the peak is slightly redshifted (Stark effect), its magnitude has decreased, and oscillations above E_g are observed. A further increase of F causes increasing amplitudes of the oscillations, a strong broadening, and a blueshift of the first peak. For $F=3F_{ion}$, this peak even occurs above E_g. The main first peak is related to the excitonic ground-state transition ($n=1$) in Elliott's model.[13] In fact, there is only a small deviation between the broadened Elliott function and the curve with $F=0.1F_{ion}$. The reason for the shift and broadening with F is the mixing of the bound state (hydrogen) wave functions with the continuum states (accelerated electrons) as the probability for the electron escape out of the Coulomb potential well created by the hole increases. It is important to note that this happens continuously with F, unlike with the classical picture. For hydrogen states with larger principal quantum number n, the critical ionization field reduces as F_{ion}/n^4, as derived from Bohr's model. For the curve with $0.1F_{ion}$ in Fig. 1, the $n=2$ state is already ionized. Thus, for GaN this state is only observable in crystal regions with $F<5$ kV/cm.

For $F=F_{ion}$ in Fig. 1, the meaning of the quantum number i and the origin of the oscillations above E_g in Blossey's model are illustrated. Each summand in Eq. (6) contributes to one bump in ε_2, where for larger i the bumps are centered

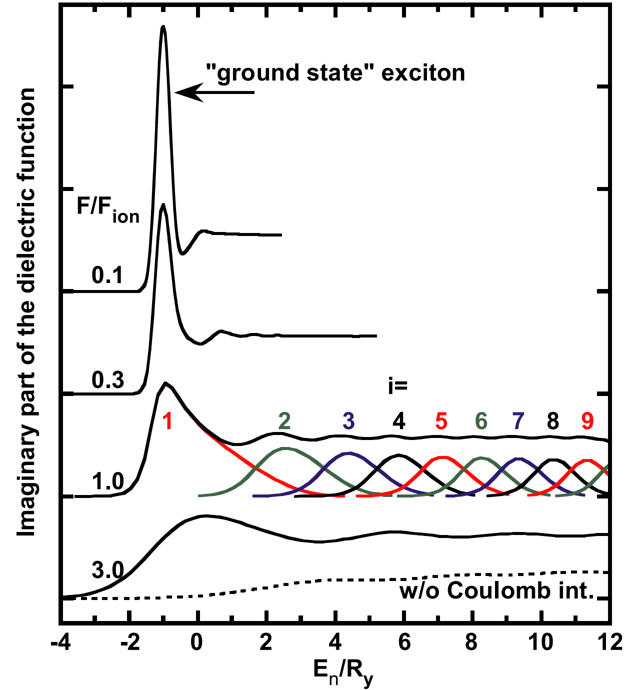

FIG. 1. (Color online) Imaginary part of the excitonic dielectric functions for electric field strengths of 0.1, 0.3, 1, and 3 times the classical ionization limit F_{ion}. The numbers at the $1.0F_{ion}$ curve refer to the quantum numbers i in Eq. (6). For $F=3F_{ion}$ the curve without Coulomb interaction is also drawn. The curves have been shifted for clarity.

at $E_n/R_y \sim \left[(F/F_{ion})\frac{3}{2}\pi\left(i-\frac{1}{2}\right)\right]^{2/3}$. In photo- and electroreflectance spectroscopy these so-called Franz-Keldysh oscillations (FKO) are detected for the determination of F. If the FKO are treated in the one-particle Franz-Keldysh picture[16,17] neglecting the Coulomb interaction, the outcome yields the same spreading of the oscillations with F, as it will be shown in Sec. IV B. However, when the full numerical calculation is compared to the single particle picture as it is shown for $F=3F_{ion}$ in Fig. 1, it is obvious that the Coulomb potential enhances not only the ε_2 magnitude around the band gap but increases also the oscillation amplitude.[3]

B. Dielectric function of GaN

We consider GaN under tensile strain, which usually occurs when growing on silicon or 6H-silicon carbide substrates. For our investigations, tensile strain is of advantage since then the FX^A resonance is not obscured by the close FX^B resonance. The reason for this is the exchange of oscillator strengths between FX^B and FX^C: under tensile strain the oscillator strength of FX^C can be as high as that of FX^A while that of FX^B goes to zero.[2] Furthermore, the increased splitting between FX^A and FX^C makes the peak assignment easier.

As the very similar Rydberg energies suggest,[1] in our calculation the contributions of the three valence bands were evaluated with equal numerical parameters. They were shifted according to the GaN strain state in our sample by the respective valence band splittings $\Delta_{AB}=3$ meV and Δ_{AC}

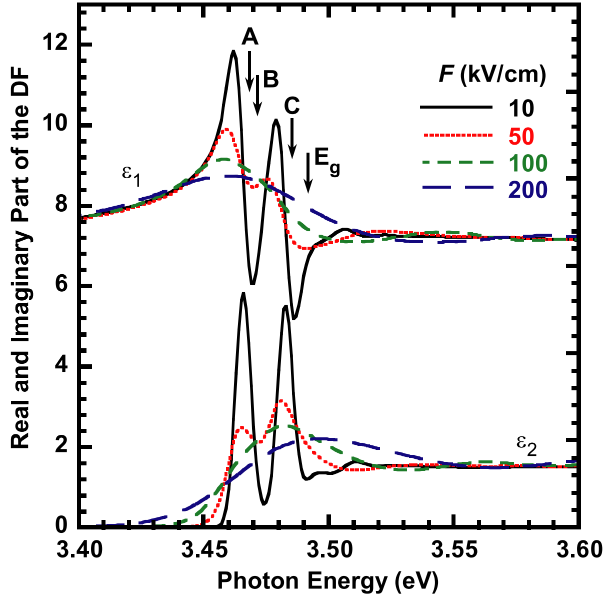

FIG. 2. (Color online) Real (ε_1) and imaginary (ε_2) parts of the dielectric function of GaN under tensile biaxial strain and at T =5 K near the band gap (E_g=3.491 eV) for electric field strengths of 10, 50, 100, and 200 kV/cm. The transition energies of the free zero-field A, B, and C excitons as well as the gap energy are marked by arrows.

=17 meV (Ref. 2) and convoluted by a Gaussian line-shape function. After this, the three contributions to ε_2 were added according to their individual (squared) matrix elements $|M_j|^2$ (j=A,B,C) describing the photon-assisted transitions with the electric field vector polarized perpendicular to the optical (c) axis (ordinary radiation). They obey a sum rule[11] and are quantified by

$$|M_j|^2 = f_j \frac{m_0}{6} E_{p\perp}, \tag{9}$$

where f_j is the fraction corresponding to one of the three valence band contributions and $E_{p\perp}$ is Kane's parameter in energy units. $E_{p\perp}$ was adjusted to 20.6 eV in order to ensure the smooth connection of the numerical results with the ellipsometrically determined $\varepsilon_2(\hbar\omega)$ from Ref. 18 above E_g. The ellipsometrical data were blueshifted by 57 meV to account for the increase of E_g at T=5 K and the tensile strain in the GaN layer of our sample. Our $E_{p\perp}$ is in close agreement to 19.8±0.5 eV reported in Ref. 10.

Although for this study the only interest lies in the region around the band gap, for a correct description of ε_1 by means of the Kramers-Kronig transformation, it was necessary to include the ε_2 data up to 9.8 eV containing the high-energy critical points of the band structure. The contributions from low photon energy processes, such as optical phonons, to ε_1 have been added by an offset corresponding to the high-frequency dielectric constant.

The real and imaginary parts of the DFs for GaN at various field strengths are presented in Fig. 2. They were calculated with the parameters given in Table I. For F=10 and 50 kV/cm clearly two resonances are observed. The feature at 3.466 eV is related to FX^A and the feature at 3.483 eV to FX^C. As F is increased, both features merge and shift to higher energies. Despite the fact that the FX^A resonance is larger for small fields, at F=200 kV/cm only a broad feature near the FX^C energy can be resolved. Also, a long absorption tail below E_g appears in ε_2. The change of ε_1 with F is only small. Since we consider GaN under tensile biaxial strain, Δ_{AB} is very low and the oscillator strength of FX^B is reduced for the benefit of FX^C. Consequently, the FX^B-related transitions are not clearly apparent in the DFs.

In Fig. 3, the F-induced shifts of the main excitonic resonances and their broadenings are demonstrated on the basis of the calculated ε_2 curves. Up to a field of ~20 kV/cm, the peaks follow the quadratic Stark shift as predicted by perturbation theory. At 40 kV/cm, a minimum is reached where the maxima lie 1.8 and 2.3 meV below the zero-field values for FX^A and FX^C, respectively. This is somewhat smaller than the unbroadened contribution of a single exciton where the maximal redshift is $0.11R_y$=2.7 meV. Above 40 kV/cm, they shift to higher energies. If one defines the difference between the peak energy and $E_g+\Delta_{AC}$ as the field-dependent Rydberg energy $\tilde{R}_y(F)$ of FX^C, we find from 200 up to the highest calculated field of 1000 kV/cm for the upper solid line a linear dependence,

$$\tilde{R}_y(F) \simeq \tfrac{1}{2}eaF - \tfrac{3}{2}R_y. \tag{10}$$

Although it was not mentioned by Blossey, the linearity is also present in a (semilogarithmic) diagram of Ref. 22. Lederman and Dow[23] support our findings by stating that the $F^{2/3}$ dependence as in the one-particle picture can only be reproduced by numerical calculations in the ultrastrong field limit,

TABLE I. Parameters for the calculation of the dielectric functions of GaN and $Al_{0.15}Ga_{0.85}N$.

Layer	E_g (eV)	$E_{p\perp}$ (eV)	f_A	f_B	f_C	μ (m_0)	ε_r	R_y (meV)	F_{ion} (kV/cm)	Γ (meV)
GaN	3.491	20.6	1[a]	0.1[a]	0.9[a]	0.197[b]	10.4[c]	25[d]	89.5	2
$Al_{0.15}Ga_{0.85}N$	3.785	22.5	1	0	1	0.212[b]	10.1[c,e]	28.4	112.2	40

[a]Reference 2.
[b]Reference 19.
[c]Reference 20.
[d]Reference 1.
[e]Reference 21.

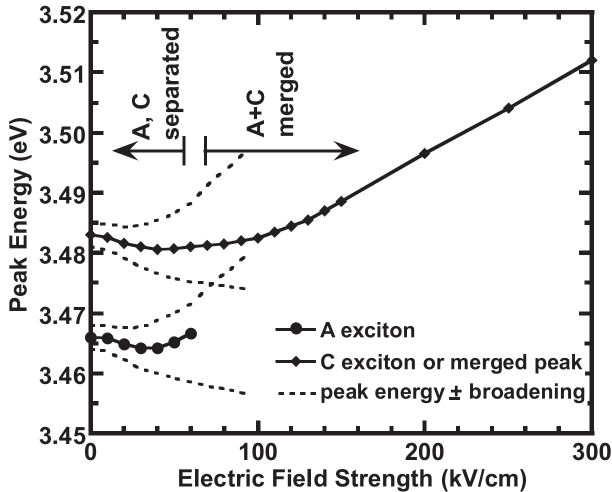

FIG. 3. Peak energies of ε_2 for the free A and the C excitons. Also shown are the peak energies plus or minus the broadening energies obtained by fitting the broadened Elliott formula to ε_2.

that is for $F/F_{ion} \geqslant 100$. Also shown is the field dependence of the broadening, which has been obtained by fitting with Gaussian broadened Elliott functions. The broadening is already field dominated above 20 kV/cm. It should be noted that the fit is rather poor for $F > 20$ kV/cm. A further increase of F leads to a merging of the A and the C peaks above 60 kV/cm. Both the peak shift and the broadening render the extraction of exciton energies, e.g., for strain evaluation, to be impossible even for $F < F_{ion}$ if the field is not properly taken into account.

The mixing of bound and continuum states with increasing F enhances α below E_g as it is shown in Fig. 4. As also predicted by the single-particle Franz-Keldysh effect,[16,17] the logarithm of α shows a dependence that is mainly governed by $(E_g - \hbar\omega)^{3/2}/F$. This is in contrast to findings of a linear dependence of $\ln(\alpha)$ from the photon energy for very low fields.[4] However, as in Ref. 4 the electron-hole interaction increases α below E_g by several orders of magnitude compared to the single-particle picture. Especially important is this effect for high-quality GaN or AlGaN layers in which, due to their large spontaneous and piezoelectric polarization charges at the heteroboundaries, fields of more than $20F_{ion}$ are typical.[24] If one likes to extract information about the material quality of such layers from the steepness of α below E_g, as it is linked to the concentration of ionized impurities by Urbach's rule,[25] one should keep in mind that the field-induced absorption dominates for large F.

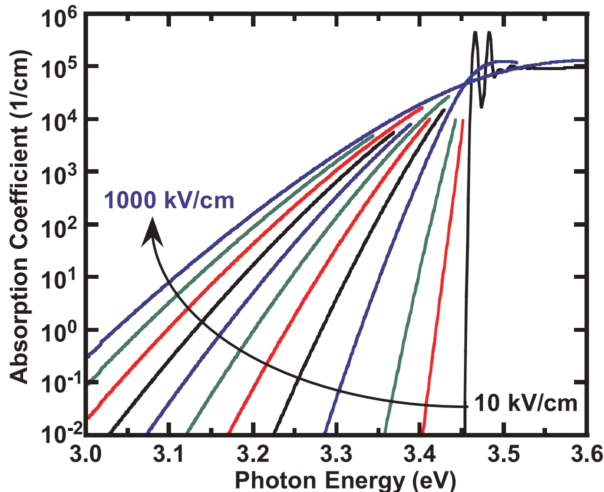

FIG. 4. (Color online) Absorption coefficient of GaN near and below the band gap at 3.491 eV for electric field strengths of 10, 50, 100, 200, 300, 400, 500, 600, 700, 800, 900, and 1000 kV/cm.

III. EXPERIMENTAL DETAILS

The theoretical calculations evidenced that the strongest influence of the electric field on the DF is expected at low F values, i.e., close to the flat band condition. It cannot be achieved by studying single nitride layers covered with a Schottky gate,[7,26] but by using AlGaN/GaN heterostructures with a two-dimensional electron gas (2DEG) present at the heteroboundary. As demonstrated recently,[24] the 2DEG can be fully depleted beneath the gate and the GaN channel layer becomes field free.

The sample studied here was grown by metalorganic vapor phase epitaxy on n-type Si(111) substrate. After the growth of a 25 nm AlN nucleation layer and a 400 nm Fe compensated GaN buffer layer, a low-temperature AlN layer (10 nm) was deposited for strain compensation. The actual heterostructure consists of about 800 nm GaN and a 22 nm thick $Al_{0.15}Ga_{0.85}N$ barrier layer, both are nominally undoped. The nitride layers have metal-face polarity. It has been confirmed by x-ray diffraction experiments at room temperature and by photoluminescence excitation spectroscopy at 5 K,[27] that the GaN is under tensile biaxial strain. As has been explained in Sec. II, tensile strain is of advantage for our experiments.

Contacts were deposited by e-beam evaporation onto the AlGaN surface and patterned by standard liftoff techniques. The ohmic contact is composed of Ti/Au/Cr/Au layers and was annealed at 800 °C. The Schottky contact has a circular geometry with a diameter of 680 μm and consists of a 10 nm thin semitransparent Pt film. As has been determined from room-temperature experiments, the 2DEG has a density of $N_{2DEG} = 1.8 \times 10^{12}$ cm^{-2} at zero bias.[28]

The ER experiments were carried out at a temperature of $T = 5$ K. A dc bias voltage U_{dc} and an added square-wave ac modulation voltage with an amplitude of $U_{ac} = 100$ mV and a frequency of 765 Hz were applied between the Schottky and the ohmic contact. The probe light was supplied by a 150 W Xe arc lamp and dispersed by a 2 m focal-length monochromator set to 2 and 10 meV spectral resolution in the ranges of 3.4–3.6 eV and 3.5–4.7 eV, respectively. Subsequently, the probe light was focused under nearly perpendicular incidence onto the Schottky contact. With lock-in technique the ER signal as the relative difference of the reflectivity R was detected, which is given by

$$\frac{\Delta R}{R}(U_{dc}) = \frac{R(U_{dc} - U_{ac}) - R(U_{dc} + U_{ac})}{R}. \tag{11}$$

Photocurrent (PC) spectra were measured with the same setup but with only dc bias and a chopper between monochromator and sample.

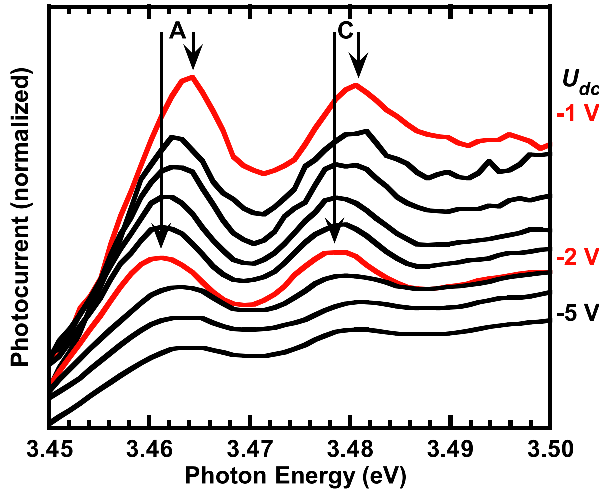

FIG. 5. (Color online) Photocurrent spectra taken at $T=5$ K near the GaN band gap for gate bias voltages of −1.0, −1.2, −1.4, −1.6, −1.8, −2.0, −3.0, −4.0, and −5.0 V. The curves have been shifted and normalized for clarity.

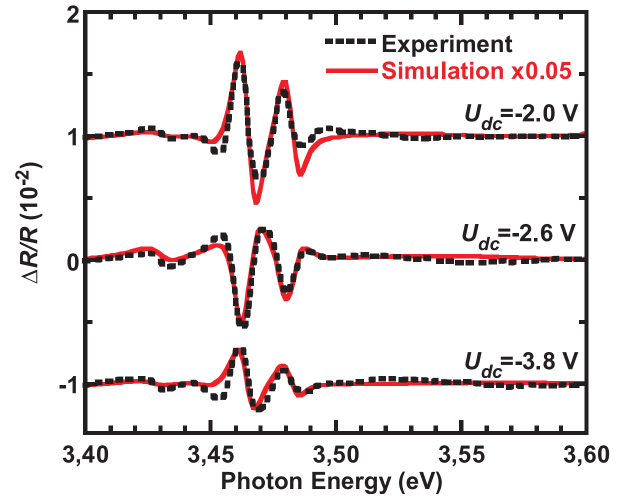

FIG. 6. (Color online) Experimental data taken at $T=5$ K and simulated ER spectra near the GaN band gap for gate bias voltages of −2.0, −2.6, and −3.8 V. The curves have been shifted for clarity.

IV. EXPERIMENTAL RESULTS AND COMPARISON TO THEORY

In this section, experimental data of the AlGaN/GaN heterostructure are compared to simulations based on the calculated DFs. PC spectroscopy at low F values demonstrates the exciton stark shift. ER measurements evidence that within the GaN a space charge region with an "exciton dead layer" (EDL) exists, characterized by $F>F_{ion}$ and a field gradient. The inhomogeneous field distribution requires the application of a multilayer model for the calculation of ER spectra. The results are compared to the experimental data taken at various voltages. At last, the influence of large homogeneous fields onto $\Delta R/R$ is studied in the region of the AlGaN band edge.

A. GaN

In Fig. 5, PC spectra for various bias voltages are shown demonstrating qualitatively the agreement of the experiment with the calculation results presented in Sec. II B. At $U_{dc}=-1$ V relatively sharp resonances for FX^A and FX^C are observed, where the height of the FX^A resonance is the largest. As it will be proved later at −1 V, the bands in the GaN are almost flat ($F \ll F_{ion}$). The decrease of U_{dc} causes the increase of F below the AlGaN/GaN interface. Consequently, the peaks broaden, their heights decrease and the height ratio between FX^A and FX^C is inverted (cf. Fig. 2). Furthermore, the low-energetic photoresponse increases (cf. Fig. 4). From $U_{dc}=-1$ V down to −2 V, the FX^A and FX^C obey the Stark effect, i.e., they shift to their lowest energies by 3.3 and 2.4 meV, respectively; below −2 V a monotonic blueshift begins (cf. Fig. 3). The experimental values for the maximal redshifts of the two bound state resonances are in good agreement to the calculated values; the blueshifts at larger negative bias (larger F) are smaller than expected. This deviation is due to the fact that the photoresponse is not identical with ε_2 it is closer related to α [see Eq. (1) for the relation between both quantities]; α shows a slightly different F dependence of the peak position. Furthermore, the photoresponse originates from the EDL in the GaN space charge region and up to now it is not clear how the individual regions of different F contribute to the photocurrent. Binet *et al.*[9] investigated this problem and observed a very large deviation between PC and absorption spectra. They pointed out that the exciton created in the first step by the absorption of a photon needs to be dissociated by the electric field and/or thermally by phonons in a second step in order to contribute to the photoconductive response.

A deeper insight into the optical properties of the GaN EDL can be obtained by ER spectroscopy. In Fig. 6, experimental spectra near the GaN band edge for three values of U_{dc} are shown [black (dashed) lines]. The most prominent features appear in contrast to the PC spectra exactly at the energies of the zero field FX^A and FX^C transitions and do not shift with U_{dc}. Note the peak shift in Fig. 3 and that at $U_{dc}=-3.8$ V F is more than three times larger than F_{ion} at the AlGaN/GaN boundary. A variation of U_{dc} merely causes a phase rotation of these features, i.e., the reversal of maxima into minima and vice versa. FKO, with comparably small magnitude whose spacing and amplitude increase with increasing reverse bias, appear above E_g. Oscillations at photon energies below E_g are also observed because the linear electro-optic or Pockels' effect is predominant.[29] The phase rotation is due to an interference phenomenon within the EDL that arises from an optical mismatch between layers with $F \ll F_{ion}$ located in the bulk and regions with large F located in the space charge region. The decrease in the amplitude of the FX^A and FX^C resonances with increasing reverse bias is due to the increase of the optical absorption as the EDL extends deeper into the bulk.[30] The voltage dependence of the rotational structure is determined by the doping level and the flat band voltage. This connection has been used to obtain both quantities for GaN Schottky diodes.[26] In contrast to the rotational structure, the FKO are caused by the large electric fields in the region just below the AlGaN/GaN interface. Only from there can the reflected high-energetic probe light exit the sample.

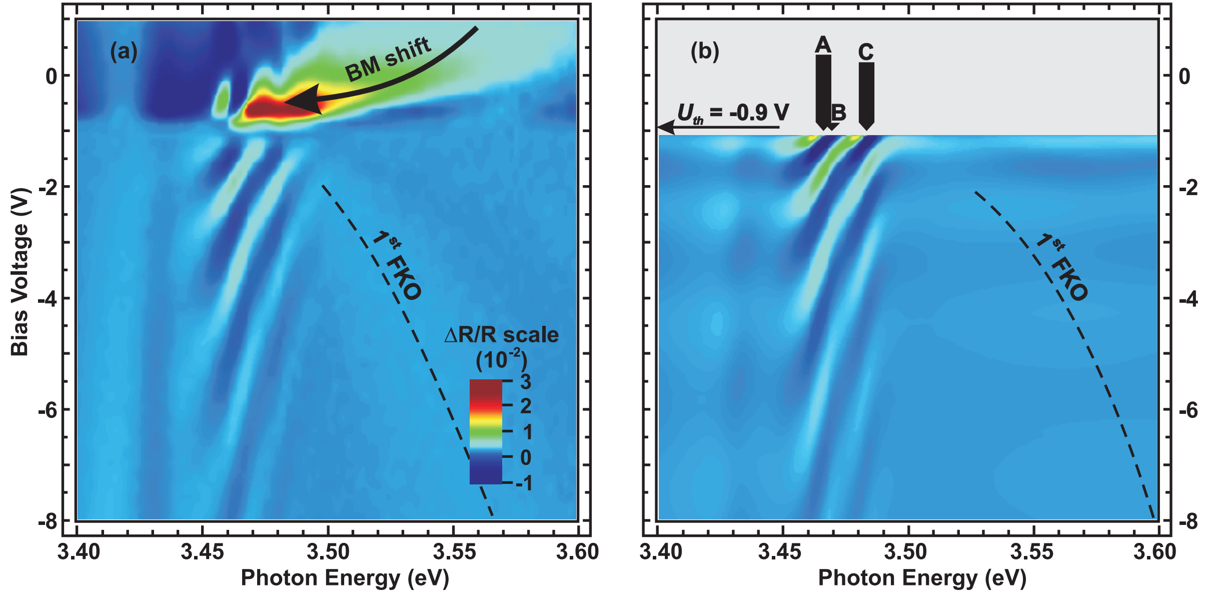

FIG. 7. (Color online) ER spectra for various gate bias voltages near the GaN band edge. Experimental data taken at $T=5$ K are shown in (a). Simulation results for bias voltages below the GaN flat band voltage of -0.9 V are shown in (b). The zero-field free excitonic transitions for the A, B, and C valence bands are indicated by arrows, their widths and heights represent the full width at half maximum (FWHM) (2Γ) and the oscillator strengths, respectively. As a guide to the eye the first maximum of the Franz-Keldysh oscillations is marked by broken lines.

With the theoretical results for the DF as a function of F, it should be possible to model the ER spectra. It is assumed in most studies that the measured $\Delta R/R$ signal [Eq. (11)] is directly related to the F-induced change of the DF by

$$\frac{\Delta R}{R}=\alpha(\varepsilon_1,\varepsilon_2)\Delta\varepsilon_1+\beta(\varepsilon_1,\varepsilon_2)\Delta\varepsilon_2, \tag{12}$$

where $\alpha(\varepsilon_1,\varepsilon_2)$ and $\beta(\varepsilon_1,\varepsilon_2)$ denote the field-independent Seraphin coefficients.[31] However, this concept cannot be applied here for two reasons. At first, the pronounced excitonic features lead to a strong photon energy dependence (usually neglected) of the coefficients. Secondly, they become field-dependent via $\varepsilon_1(F)$ and $\varepsilon_2(F)$, as shown in Fig. 2. Additionally, the electric field in the GaN layer is inhomogeneous causing a spatial varying DF. Under those conditions, the ER signal can be calculated by a multilayer approach[32,33] by dividing the space charge region into thin layers of GaN characterized by DFs with the appropriate field strengths. The stack is built up as follows: vacuum, Pt (10 nm), AlGaN ($d_{\mathrm{AlGaN}}=22$ nm), the GaN space charge region of width z_{sc}, the GaN bulk with $F=0$ of width $1170\ \mathrm{nm}-z_{\mathrm{sc}}$, and at last the Si substrate. The thin buried AlN layers were disregarded because the GaN layer on top is much thicker than the light penetration depth. Moreover, the AlN DF is not modulated by the applied voltage. Vacuum and substrate were taken semi-infinitely. The AlGaN DF has been obtained by energy-shifted ellipsometrical data taken at room temperature from the same sample. In the space charge region, F decreases stepwise from F_{hb} at the AlGaN/GaN heteroboundary down to zero in steps of 2 kV/cm. The quantities z_{sc} and F_{hb} are controlled by the applied voltage $U=U_{\mathrm{dc}}\pm U_{\mathrm{ac}}$,

$$z_{sc}=\sqrt{-\frac{2\varepsilon_0\varepsilon_r}{eN_D^+}\varphi}, \tag{13a}$$

$$F_{hb}=\frac{eN_D^+}{\varepsilon_0\varepsilon_r}z_{sc}, \tag{13b}$$

where the electrostatic potential for electrons at the boundary is $\varphi\simeq U-U_{th}-F_{hb}d_{\mathrm{AlGaN}}$, it incorporates the potential drop over the AlGaN barrier. For the donor density in the GaN a value of $N_D^+=1.2\times10^{17}\ \mathrm{cm}^{-2}$ was chosen, so that the experimentally observed phase shift of the ER signal with U_{dc} was reproduced. Note that this specific value overestimates the real one because the sample is highly resistive at a temperature of 5 K and a voltage drop, e.g., in the GaN bulk or the contacts, acts in the same manner. This interpretation is supported by the small inhomogeneous broadening needed for the simulation. $U_{th}=-0.9$ V is the GaN flat band voltage, see below. With these values and $U_{\mathrm{dc}}=-8$ V, F_{hb} and z_{sc} amount to 498 kV/cm and 239 nm, respectively. The simulation results are also shown in Fig. 6; besides a common scaling factor (which accounts for such effects as lateral sample inhomogeneities, probe beam divergence, or capacitive charge transfer), the curves are in very good agreement to the experimental data.

Figure 7(a) shows a U_{dc} map of the experimental ER spectra taken around the GaN band gap for the whole investigated range from $1\ \mathrm{V}\geqslant U_{\mathrm{dc}}\geqslant-8$ V. Obviously, the principal behavior changes drastically at the threshold voltage of $U_{th}=-0.9$ V corresponding to flat band condition in the GaN layer (see Ref. 24, and references therein). Toward positive gate voltages, a 2DEG with increasing density is formed beneath the AlGaN/GaN heteroboundary. The increasing band-

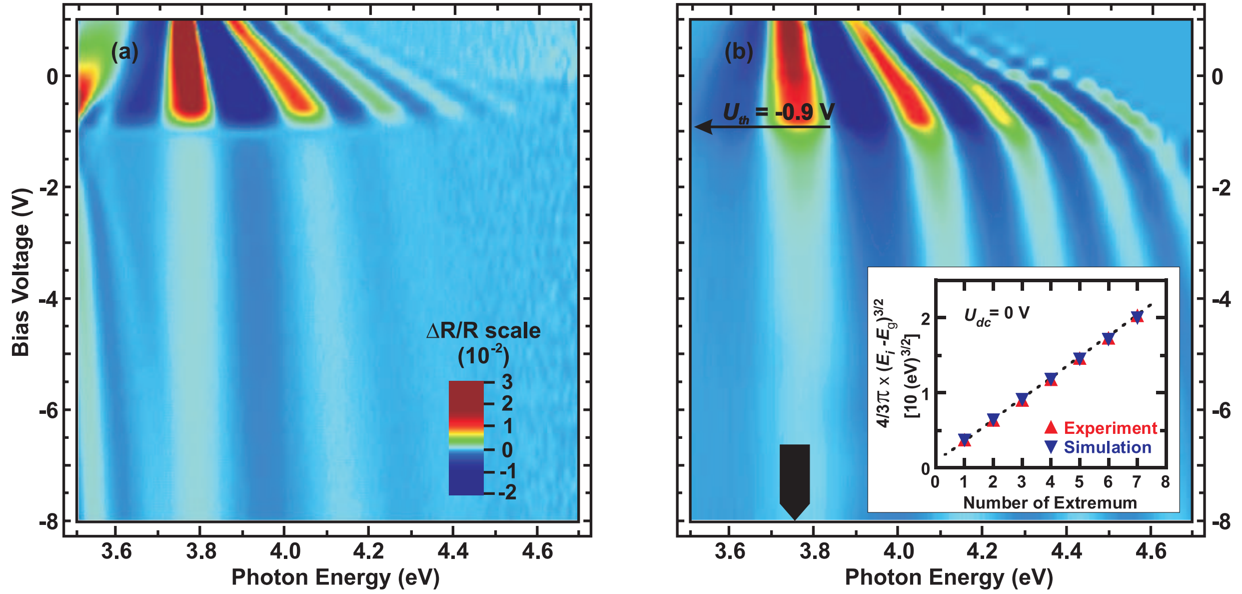

FIG. 8. (Color online) ER spectra for various gate bias voltages near the $Al_{0.15}Ga_{0.85}N$ band edge. Experimental data taken at $T=5$ K are shown in (a). Simulation results are presented in (b), the inset shows a comparison to experimental data at 0 V bias. The arrow at the bottom represents the zero-field excitonic transition energy and its FWHM (2Γ). The inset shows the position E_j of the FKO extrema vs their number.

filling leads in a spatial restricted region of the GaN channel layer to a shift of the absorption edge to higher energies, which is also known as Burstein-Moss (BM) shift. The applied modulation voltage causes a change of the 2DEG density and therefore of the position of the steplike absorption edge of the quasi-two-dimensional system. As a result, a strong maximum of the ER spectra is observed that is unambiguously related to the BM shift. Calculated $\Delta R/R$ spectra for the range of 2DEG formation ($U_{\mathrm{dc}} > U_{th}$) cannot be given at present because it requires a DF calculation, which includes the effects of band filling, band gap renormalization, and carrier density-dependent exciton screening.

For more negative voltages ($U_{\mathrm{dc}} < U_{th}$), no 2DEG exists and the optical response of the structure has to be discussed in terms of the above calculated DF only, i.e., with electron-hole interaction. The experimental ER map in this range [Fig. 7(a)] exhibits a number of sharp maxima and minima that undergo an apparent shift to lower energies when U_{dc} is decreased. The origin of this peculiarity becomes clear from a comparison to the theoretical ER results. The calculation was carried out with the approach explained above, i.e., with inhomogeneous field distribution. The results are presented in Fig. 7(b); they fully reproduce the experimental data. It emphasizes the accuracy of the calculated DFs. Since the field free exciton positions were fixed in the simulation, the $\Delta R/R$ extrema shift is not caused by a shift of an electronic state. It is attributed to interference within the EDL and the change of the EDL width. It should be noted that $\Delta R/R$ has a zero crossing at the positions of the field-free A and C excitonic ground states for $U_{\mathrm{dc}} = U_{th}$.

In both spectral maps, the first maximum of the FKO evolves to higher photon energies with increasing reverse bias. These features are very weak and are emphasized by the respective broken lines in Figs. 7(a) and 7(b). In the experiment a ridge appears, whereas in the simulation a range of hills is present interrupted by valleys every time a full rotation of the FX^A and FX^C resonances has been completed. We attribute this difference between experiment and simulation to the same reasons that cause the scaling of $\Delta R/R$. When comparing both maps, the first FKO occurs at higher energies and has a stronger voltage dependence in the simulation. The large value of F_{hb} gives rise to this feature. The observed difference is caused by an overestimated F_{hb} due to the overestimated N_D^+ in the simulation.

B. AlGaN

It is also of interest to study the optical properties of the AlGaN layer because its electric field is much larger than that of the GaN. The reason for this is the large difference between the AlGaN and GaN macroscopic polarizations P^{AlGaN} and P^{GaN}, respectively. The polarizations include a spontaneous part due to the lack of inversion symmetry of the wurtzite crystal and a piezoelectric part due to layer strain.[34] The discontinuity at the heteroboundary acts like an interface charge, and thus, the absolute value of the AlGaN field is given by

$$F = \frac{1}{\varepsilon_0 \varepsilon_r^{\mathrm{AlGaN}}} (\varepsilon_0 \varepsilon_r^{\mathrm{GaN}} F_{hb} + |P^{\mathrm{AlGaN}} - P^{\mathrm{GaN}}|). \qquad (14)$$

Figure 8(a) shows a U_{dc} map of ER spectra in the spectral region of the AlGaN band gap. Below 3.6 eV, features from the GaN are observed. At about 3.76 eV, a first maximum originating from the AlGaN appears, which is followed by the FKOs. This peak lies slightly below the presumed AlGaN band gap; it shifts by about 20 meV to higher energies and broadens as the voltage is decreased. Individual contributions of the three excitons cannot be resolved due to the

field-induced broadening (see Fig. 3). From +1 V to U_{th}, an increasing period of the FKOs is observed, indicating an increasing F. Below U_{th}, the ER signal decreases drastically and the spreading of the FKO increases only slightly. This behavior is due to the complete depletion of the 2DEG. In this U_{dc} range, the most part of the modulation voltage drops off in the GaN space charge layer.

In order to simulate the ER signal, the F-dependent DF for $Al_{0.15}Ga_{0.85}N$ has to be calculated in a similar way as explained for the GaN in Sec. IV A. It is necessary to know the electric field strength and its modulation under the experimental conditions as input parameters. Using Aspnes' asymptotic expression for the FKO,[35] the $F(U_{\mathrm{dc}})$ dependence was obtained (the verification of the values will be given below): from 1 V down to U_{th} F increases linearly from 310 kV/cm up to 920 kV/cm and increases further up to 1350 kV/cm at −8 V. The field modulation below U_{th} is given by $\pm U_{\mathrm{ac}}/d_{\mathrm{AlGaN}}=\pm 45$ kV/cm, assuming a total pinning of the conduction band edge at the AlGaN/GaN heteroboundary by the 2DEG. Above U_{th}, the same modulation as that of F_{hb} in Eq. (13) was taken.

Assuming a linear dependence of the crystal field energy on the Al content, one obtains for $Al_{0.15}Ga_{0.85}N$ a negative crystal field of $\Delta_{cf}=-26$ meV from the values of 10 meV (Ref. 2) and −230 meV (Ref. 36) for GaN and AlN, respectively. The corresponding split off energies Δ_{so} amount to 18 meV (Ref. 2) and 19 meV (Ref. 37). Because of the negative Δ_{cf}, the uppermost valence band of the alloy has Γ^7 symmetry but the calculated oscillator strength for the polarization $\mathbf{E}\perp c$ is already very low without strain. The strong tensile strain reduces this value further. Therefore, its relative contribution f_{B} is set to zero, and the two other oscillator strengths become equal. The splitting between the corresponding valence bands amounts to only $\Delta_{AC}=14$ meV. Because the value is much smaller than the F-induced broadening of the DF, the splitting was neglected ($\Delta_{AC}=0$). $E_{P\perp}$ was adjusted to 22.6 eV to align the calculated results with the energy-shifted experimental data of the same sample measured by ellipsometry at room temperature. The set of parameters used is given in Table I.

For the simulation of $\Delta R/R$, a similar optical layer model as in Sec. IV A was created but without electric field in the GaN layer neglecting the small influence of the 2DEG[38] for $U_{\mathrm{dc}}>U_{th}$ and the field-induced change of the GaN DF for $U_{\mathrm{dc}}<U_{th}$. The results presented in Fig. 8(b) show the good agreement to the experimental data. However, the magnitude in the calculation does not decrease as strong with $\hbar\omega$ as in the experimental data. One reason for this is that for photon energies larger than E_g, the broadening parameter Γ should increase with the photon energy[39] resulting in a faster decrease of $\Delta R/R$. The increasing nonparabolicity of the conduction band with increasing energy results in a further damping of the oscillations.

Since Aspnes' method for the evaluation of the FKO to obtain F was used, it is important to know how large the error in F is due to the disregard of the Coulomb interaction. The inset in Fig. 8(b) shows, for the experimental and simulation data at $U_{\mathrm{dc}}=0$ V, the position of the FKO extrema E_j plotted as $(4/3\pi)(E_j-E_g)^{3/2}$ vs the number of the extremum j. The slope of the experimental data yielded an F of 641 ± 7 kV/cm, whereas for the simulation, 637 ± 2 kV/cm was obtained. Similar investigations were performed in the range of $F=F_{ion}/2$ up to $5F_{ion}$ by comparing the FKO extrema obtained from Aspnes' expression to that from the full numerical calculation. They also show that for the determination of F the Coulomb interaction can be neglected; the deviations lie typically below 2%.

V. CONCLUSIONS

The linear optical properties of wurtzite nitrides characterized by the complex DF were calculated in the vicinity of the band gap, where excitons play a major role. The influence of electric fields on the optical response was theoretically studied and compared to experimental data.

The theoretical approach based on Blossey's theory yielded the imaginary part of the DF by the exact numerical solution of the hydrogen problem in a constant electric field in the whole range of reasonable field strengths. The contributions of the three valence bands were treated separately. The real part of the DF was obtained by the Kramers-Kronig transformation, including the low-energy background and high-energy critical points of the band structure.

For the example of GaN, it was shown how the electric field influences position, magnitude, and broadening of the exciton ground state resonance. In contrast to the one-electron picture, for large fields a linear shift of the energy position of the exciton ground-state resonance with F was obtained. Furthermore, the F-dependent absorption coefficient below the band gap has been calculated, which is of importance for the evaluation of material quality from absorption experiments and for the improvement of laser diodes and nonlinear devices.

ER spectroscopy of an AlGaN/GaN heterojunction at low temperatures demonstrated the sensitivity of the optical response to field changes. At first the ER spectra of the GaN channel layer were simulated by means of the calculated field-dependent values of the DF and an optical multilayer model. Despite the influences of the lateral field inhomogeneity, excellent agreement between experiment and theory was obtained. Second, the very large homogeneous field in the $Al_{0.15}Ga_{0.85}N$ top layer allowed us to study the field-induced fluctuations of the excitonic density of states observable as the FKO in the ER spectra. Although the experimental data could be well reproduced by our DF model, it was found that for the determination of F by the analysis of the FKO extrema the simple one-particle picture is still applicable.

ACKNOWLEDGMENTS

We would like to thank Olaf Weidemann and Martin Eickhoff for the processing of the contacts, Philipp Maaß for fruitful discussions, and Henning Schwanbeck for the help with the computing facilities. The group at Ilmenau acknowledges the financial support by the Deutsche Forschungsgemeinschaft (Grant No. KR2228/3-2).

*Electronic address: Ruediger.Goldhahn@tu-ilmenau.de

[1] K. Kornitzer, T. Ebner, K. Thonke, R. Sauer, C. Kirchner, V. Schwegler, M. Kamp, M. Leszczynski, I. Grzegory, and S. Porowski, Phys. Rev. B **60**, 1471 (1999).
[2] B. Gil, in *Gallium Nitride (GaN) II*, edited by J. I. Pankove and T. D. Moustakas (Academic Press, New York, 1999), pp. 209–273.
[3] D. F. Blossey, Phys. Rev. B **2**, 3976 (1970).
[4] J. D. Dow and D. Redfield, Phys. Rev. B **1**, 3358 (1970).
[5] L. Schultheis and I. Balslev, Phys. Rev. B **28**, 2292 (1983).
[6] P. Trautman, K. Pakula, R. Bozek, and J. Baranowski, Appl. Phys. Lett. **83**, 3510 (2003).
[7] S. Shokhovets, D. Fuhrmann, R. Goldhahn, G. Gobsch, O. Ambacher, M. Hermann, and U. Karrer, Phys. Status Solidi A **194**, 480 (2002).
[8] A. Oberhofer, J. Muth, M. Johnson, Z. Chen, E. Fleet, and G. Cooper, Appl. Phys. Lett. **83**, 2748 (2003).
[9] F. Binet, J. Y. Duboz, E. Rosencher, F. Scholz, and V. Härle, Phys. Rev. B **54**, 8116 (1996).
[10] S. Shokhovets, G. Gobsch, and O. Ambacher, Appl. Phys. Lett. **86**, 161908 (2005).
[11] Yu. M. Sirenko, J. B. Jeon, B. C. Lee, K. W. Kim, M. A. Littlejohn, M. A. Stroscio, and G. J. Iafrate, Phys. Rev. B **55**, 4360 (1997).
[12] For example, see S. L. Chuang, *Physics of Optoelectronic Devices* (Wiley, New York, 1995).
[13] R. J. Elliott, Phys. Rev. **108**, 1384 (1957).
[14] S. Wolfram, *The Mathematica Book* (Wolfram Media, Champaign, 2003).
[15] For example, see P. Harrison, *Quantum Wells, Wires and Dots* (Wiley, New York, 2000).
[16] W. Franz, Z. Naturforsch. A **13**, 484 (1958).
[17] L. V. Keldysh, Sov. Phys. JETP **7**, 788 (1958).
[18] C. Buchheim, R. Goldhahn, M. Rakel, C. Cobet, N. Esser, U. Rossow, D. Fuhrmann, and A. Hangleiter, Phys. Status Solidi B **242**, 2610 (2005).
[19] I. Vurgaftman and J. R. Meyer, J. Appl. Phys. **94**, 3675 (2003).
[20] A. S. Barker and M. Ilegems, Phys. Rev. B **7**, 743 (1973).
[21] Y. Goldberg, in *Properties of Advanced Semiconductor Materials GaN, AlN, InN, BN, SiC, SiGe*, edited by M. E. Levinshtein, S. L. Rumyantsev, and S. M. Shur (Wiley, New York, 2001), pp. 31–47.
[22] D. F. Blossey, Phys. Rev. B **3**, 1382 (1971).
[23] F. L. Lederman and J. D. Dow, Phys. Rev. B **13**, 1633 (1976).
[24] A. T. Winzer, R. Goldhahn, G. Gobsch, A. Link, M. Eickhoff, U. Rossow, and A. Hangleiter, Appl. Phys. Lett. **86**, 181912 (2005).
[25] J. D. Dow and D. Redfield, Phys. Rev. B **5**, 594 (1972).
[26] S. Shokhovets, D. Fuhrmann, R. Goldhahn, G. Gobsch, O. Ambacher, M. Hermann, U. Karrer, and M. Eickhoff, Appl. Phys. Lett. **82**, 1712 (2003).
[27] A. T. Winzer, R. Goldhahn, G. Gobsch, A. Dadgar, H. Witte, A. Krtschil, and A. Krost, Superlattices Microstruct. **36**, 693 (2005).
[28] A. Winzer, R. Goldhahn, G. Gobsch, A. Dadgar, A. Krost, O. Weidemann, M. Stutzmann, and M. Eickhoff, Appl. Phys. Lett. **88**, 024101 (2006).
[29] S. Shokhovets, R. Goldhahn, and G. Gobsch, Mater. Sci. Eng., B **93**, 215 (2002).
[30] D. E. Aspnes and A. A. Studna, Phys. Rev. B **7**, 4605 (1973).
[31] B. O. Seraphin and N. Bottka, Phys. Rev. **145**, 628 (1966).
[32] L. Schultheis and J. Lagois, Phys. Rev. B **29**, 6784 (1984).
[33] U. Behn and H. Röppischer, Phys. Status Solidi B **141**, 325 (1987).
[34] O. Ambacher, J. Majewski, C. Miskys, A. Link, M. Hermann, M. Eickhoff, M. Stutzmann, F. Bernardini, V. Fiorentini, V. Tilak, B. Schaff, and L. F. Eastman, J. Phys.: Condens. Matter **14**, 3399 (2002).
[35] D. E. Aspnes, Phys. Rev. B **10**, 4228 (1974).
[36] L. Chen, B. J. Skromme, R. F. Dalmau, R. Schlesser, Z. Sitar, C. Chen, W. Sun, J. Yang, M. A. Khan, M. L. Nakarmi, J. Y. Lin, and H.-X. Jiang, Appl. Phys. Lett. **85**, 4334 (2004).
[37] P. Carrier and S.-H. Wei, J. Appl. Phys. **97**, 033707 (2005).
[38] B. Jogai, Phys. Status Solidi B **241**, 952 (2004).
[39] A. Jaeger and G. Weiser, Phys. Rev. B **58**, 10674 (1998).